Applied Surface Science 600 (2022) 154078

Contents lists available at ScienceDirect

Applied Surface Science

journal homepage: www.elsevier.com/locate/apsusc

Full Length Article

Signatures of bright-to-dark exciton conversion in corrugated MoS_2 monolayers

Maciej Wiesner [a,b,f,*], Richard H. Roberts [b,c], Ruijing Ge [b,c], Lukas Mennel [d], Thomas Mueller [d], Jung-Fu Lin [c,e], Deji Akinwande [b,c], Jacek Jenczyk [f]

[a] Faculty of Physics, Adam Mickiewicz University, Uniwersytetu Poznanskiego 2, PL61614 Poznan, Poland
[b] Microelectronics Research Center, The University of Texas at Austin, Austin, TX 78757, USA
[c] Texas Materials Institute, The University of Texas at Austin, Austin, TX 78757, USA
[d] Vienna University of Technology, Institute of Photonics, Gußhausstraße 27-29, 1040 Vienna, Austria
[e] Department of Geological Sciences, Jackson School of Geosciences, The University of Texas at Austin, Austin, TX 78712, USA
[f] NanoBioMedical Centre, Adam Mickiewicz University, Wszechnicy Piastowskiej 3, PL 61614 Poznan, Poland

ARTICLE INFO

Keywords:
Molybdenum disulphide
Periodic potential
Exciton
Spin flip
Bandgap anisotropy
Exciton conversion

ABSTRACT

In this study, we investigated the effect of periodic uniaxial strains on electron and phonon transports of polycrystalline and single-crystal molybdenum disulphide (MoS_2) monolayers on a periodically corrugated sapphire surface. Analysis of micro-Raman, polarized photoluminescence and second harmonic generation results shows the anisotropy of the corrugation-induced strain in both single- and polycrystalline MoS_2 monolayers. AFM topography measurements show periodically-rippled surfaces of the MoS_2 in the nanometre scale. Our results show that the application of the periodic strain produces two major effects on the band structure of MoS_2 monolayers: modulations on the band gap anisotropy and reduction of out-of-plane spin-relaxation time due to substrate-induced bending of MoS_2. Spin memory loss, in other words, shortening the spin relaxation time, enables an electron spin-flip scattering process that can convert a formerly bright exciton to a dark exciton. Such conversion is reflected in decreasing intensity of photoluminescence and in the light intensity collected by scanning near-field microscope. Our results demonstrate the ability to control both the bandgap and exciton character in monolayer MoS_2 via periodic strains imposed by corrugated sapphire substrates. This approach offers an effective means in designing novel electronic devices for photovoltaic applications. The bright-to-dark excitons conversion in photovoltaic devices can boast longer lifetimes than their bright exciton counterparts so they can be more efficiently collected by external electrodes. The strain-induced conversion of the bright-to-dark excitons makes the hybrid MoS_2/corrugated sapphire structure an interesting platform for future photovoltaic applications.

1. Introduction

The vastly increasing rate of global energy consumption is a driver for the fabrication of renewable energy sources, and immense efforts have been devoted to reducing our dependency on fossil fuels. Recently, considerable progress has been made in the fabrication of flexible nanoelectronic devices for energy harvesting and medical applications [1,2]. Photovoltaic devices are one of the most promising energy converters, and material selection for such devices requires careful matching of bandgap energy, excited carrier (exciton) lifetimes, and wavelengths of absorbed light.

Contemporary materials used for fabrication of photovoltaic devices have well-defined bandgaps and typically convert only a narrow range of wavelengths into a current. Crucially, a large mismatch between the incident photon energy and the width of the bandgap results in energy loss in form of heat. Another difficulty to overcome in photovoltaic devices is the short lifetime of excitons, as high collection efficiency of the photo-generated electron-hole pairs (excitons) requires long lifetimes and high mobility of the charge carriers in the material. Two factors have been considered to extend an exciton's life time: short

* Corresponding author.
E-mail addresses: mwiesner@amu.edu.pl (M. Wiesner), rhroberts@utexas.edu (R.H. Roberts), lukas.mennel@tuwien.ac.at (L. Mennel), thomas.mueller@tuwien.ac.at (T. Mueller), afu@jsg.utexas.edu (J.-F. Lin), deji@ece.utexas.edu (D. Akinwande), jacjen@amu.edu.pl (J. Jenczyk).

https://doi.org/10.1016/j.apsusc.2022.154078
Received 22 March 2022; Received in revised form 13 June 2022; Accepted 24 June 2022
Available online 2 July 2022

localization length [3], for example due to a strain application [4] and thermal stabilisation at higher temperatures [5]. The above mentioned processes refer mostly to bright excitons (their recombination is accompanied by light emission). However, there is another type of quasiparticles – dark excitons [6] with much longer lifetime. Conversion from bright to dark excitons may thus offer another solution for increasing the efficiency of photovoltaic devices.

The monolayer transition metal dichalcogenide (TMD) MoS_2 is characterised by electron mobilities reaching 217 $cm^2V^{-1}s^{-1}$, a satisfactory Young modulus of 0.33 TPa [7,8] and power conversion efficiency of about 5% in photovoltaic applications [9]. It possesses an (optical) bandgap of 1.86 eV. The direct band gap is located at the edges of hexagonal Brillouin zone, at the non-equivalent valleys K ±. Due to the spin–orbit (SO) interactions, each valley is spin-split, what results in two distinct exciton resonances. First can be excited by light and is composed of an electron from one of the two conduction bands (split by the SO interaction) and a hole from the upper valence band. Because these electrons and holes have parallel spin orientations, they are optically active and are called bright excitons (radiative recombination). Their lifetimes, typically about 10^{-1}ps, can be extended due to the excitons' strong localisation. Localization increases with increasing temperature, and can also be spatially controlled by strain introduced via nanostructures on which the monolayer is transferred. The spatial localization is described by the localization length L_c. For MoS_2 at a given temperature and $L_c < 100$ nm, exciton lifetimes can be increased by four orders of magnitude compared with those for $L_c > 100$ nm [3].

Second type of excitons consist of electrons and holes of antiparallel spin orientation which form so called spin-forbidden dark states (non-radiative recombination) [10,11,12,13,14,15]. Due to momentum conservation, they cannot be excited by light. However, they can be generated by the scattering of bright excitons into lower energy states, which are 14 meV below bright once [16].

Previous studies on MoS_2 have shown that tensile (compressive) strain reduces (increases) the bandgap energy [17,18]. The bandgap modification is linear with decreasing strain for small tensile strains (≪1%), non-linear for larger strains [19], and shows both a direct–to–indirect bandgap transition and semiconductor–to–metal transition for tensile strain ≫1% [10]. Valence and conduction band splitting [13] and enhanced exciton-phonon coupling (leading to intervalley scattering of charge carriers) [20] have also been observed with increasing tensile strain. In device applications, bilayer MoS_2 field-effect transistors (FET) show significant improvement in charge mobility and on-current density in a strain-gated geometry [21,22,23]. Recent investigations of electronic properties of MoS_2 coupled with a strain–inducing periodic nanostructure have revealed doping and Fermi level modulations with respect to the peaks and troughs of a corrugated nanostructure [24].

Herein, we discuss another effect of strain on excitons' behaviour, which may lead to the conversion of bright to dark excitons and as a result extending exciton's lifetime. The conversion at room temperature was reported in ref. 20 as a result of scattered of bright excitons by phonons from the KK state to dark excitons at the KΓ state (K-point for an electron and Γ-point for a hole), because the KΓ state lies energetically below the KK exciton state. Such a process is manifested in photoluminescence (PL) measurements as a change of PL intensity. Zhu et. al. observed this phenomenon and attributed it to intervalley scattering from the K-point to the spin–degenerate Γ-point [25]. Previously the photoluminescence change was attributed to the indirect bandgap, which emergence has been reported for strains>1% [10,26].

Importantly, a recent theoretical work [27] reported that the application of strain can lead to the reduction of electrons' spin memory, the reduction of spin-relaxation time of electrons as a result of spin–lattice coupling. According to the paper, the coupling parameter depends on spin-phonon interaction and local curvature tensor. The parameter has two components: one along the z-direction and another (inhomogeneous) in the *xy* plane. The second component depends on the local curvature tensor of the bended MoS_2 and is responsible for the spin–lattice relaxation phenomenon.

Motivated by the theoretical work, we designed experiments to use a periodically corrugated sapphire surface as a substrate with local curvature to enhance the spin–lattice coupling of MoS_2 monolayer and as a result, reduce its spin relaxation time. This periodic strain on the corrugated substrate induces bending of MoS_2. Electrons moving across such bended surface loses their spin memory (the spin relaxation phenomenon) which could enable an electron spin-flip scattering process.

Energy change of the electron related with the spin-flip requires band degeneracy. The degeneracy can be lifted by a strong spin–orbit interaction or by application of uniaxial strain. Specifically, the spin–orbit coupling is responsible for the degeneracy of spin states in the valence band, giving rise to well separated A and B excitonic transitions where the energy difference between A and B excitons is a measure of the valence band splitting. Such mechanism involving the spin-relaxation and band degeneracy phenomena can lead to bright to dark excitons conversion.

The nano–corrugated substrate is used to introduce strain on MoS_2 to modify its band gap [10,11,12,26,28,29]. We should also mention that applied strain leads to spatial localization of excitons (the funnel effect [11,30,31,32]). To date, however, there is little experimental data reporting the degeneracy of the band structure at K and K' points of the Brillouin zone and its effect on excitons dynamics.

In this work we have investigated the effect of strain and spin–lattice coupling on excitons dynamics to verify the phenomenon about spin-flip of electrons or holes. The possibility of generating nanostructure-induced conversion of excitons opens the door for a variety of applications in atomically thin materials including photovoltaics, quantum optics, and two-dimensional optoelectronic and nanoelectronic devices.

2. Methods

2.1. Sample preparation

Polycrystalline and single-crystal MoS_2 monolayers were used as the starting samples for the experiments. Both samples were transferred onto corrugated as well as flat sapphire substrates in order to evaluate how the periodic strain affects the samples' transport properties. M-plane $[10\bar{1}0]$ cut sapphire single crystals (α-Al_2O_3) were commercially purchased from CrysTec GmBH. The corrugated sapphire surface (Figure S1) was fabricated via reconstruction of the crystallographic planes of the substrate when subjected to a special heat–treatment procedure [33,34,35]. The M-plane sapphire surface became unstable when annealed at high temperatures (T > 1400 °C) and underwent spontaneous faceting leading to V-shaped nanogrooves formation with corrugated surfaces that are desirable for the experiments. In order to reconstruct the sapphire surface, an HTF Carbolite high–temperature chamber furnace was utilized to treat the substrate at maximum operating temperatures up to 1700 °C. Depending on annealing time (between 12 h and 22 h) and temperature (1450 ^{0}C and 1550 ^{0}C), the corrugation period and height of the sapphire substrates varied from 180 nm to 250 nm and from 10 nm to 20 nm, respectively. The polycrystalline and single-crystal MoS_2 monolayers were then transferred onto the corrugated and flat sapphire substrates using the PDMS and wet-transfer techniques, respectively.

3. Experiment

Raman and PL experiments were conducted using a commercial Renishaw *inVia* micro-Raman system equipped with a 473-nm wavelength laser and a CCD in Mineral Physics Laboratory of the University of Texas at Austin. All Raman spectra were measured using a 50 × objective resulting in a focused beam spot ~1 um in diameter and ~3 mW of the laser power at the sample surface. The Raman spectral resolution of

~1 cm^{-1} was achieved using a 2400 l/mm grating and a Renishaw 1″ CCD array with 1024 × 256 pixels. For polarized PL measurements, the incident laser had an established polarization angle with respect to the samples and only PL signals with polarizations parallel to the incident beam polarization were collected (Fig. 1a). The samples were rotated with respect to the incident polarization via a motorized rotation stage and a DC servo motor controller purchased from ThorLabs. Initial PL mapping was used to select an area of the largest PL intensity and then PL and micro-Raman anisotropy response was measured as a function of the angle between the incident polarization direction and the corrugation orientation (Fig. 1a).

The scanning near-field optical microscopy (SNOM) measurements were further conducted on the samples to relate the highest intensity of emitted light by recombining excitons with the MoS_2 topography. A commercial NT-MDT system in the reflection mode is combined with the SNOM and shear force microscopy (SFM) techniques at the Nano-BioMedical Centre in Poznan, Poland for the experiments. SFM was used to bring an optical fibre to the proximity of the sample in order to scan its surface. To excite excitons in MoS_2 monolayers, a laser with wavelength $\lambda = 488$ nm was delivered by an optical fibre with metallic end diameter $d \ll \lambda$. Emitted light was collected by far-field optics and delivered to a photomultiplier for the spectrum collection and analysis.

4. Results

Bulk MoS_2 consists of periodically stacked S–Mo–S layers bonded together by van der Waals forces. Each MoS_2 monolayer in single–crystal and polycrystalline forms displays two characteristic Raman vibrations – the E^1_{2g} mode at 385.6 cm^{-1} and A_{1g} mode at 404.9 cm^{-1} – and one PL peak at 1.86 eV corresponding to its optical bandgap [36]. The double-degenerate E^1_{2g} mode is attributed to the in-plane relative motion between the two adjacent S atoms and the Mo atom, whereas the A_{1g} mode is attributed to the out-of-plane vibration of the two S atoms in opposite directions [37].

Raman and PL spectra of the single– and polycrystalline MoS_2 monolayers on flat sapphire substrates with periods of 180 nm and 250 nm were used as nominally zero-strain references, and are presented in Figure S2. Analysis of their Raman peak positions presented in Table S1 and Table S2 confirms that strain in the reference samples was indeed negligible. The frequency difference between the E^1_{2g} and A_{1g} modes is < 19 cm^{-1} which confirms the monolayer thickness of the MoS_2 samples [29,38,39]. On the other hand, the absence of the E_{2g} mode splitting as well as the lack of an anomaly in the dependence of the micro-Raman shift of the E_{2g} and A_{1g} vibrational modes vs. the angle α between polarization of the incident laser beam and corrugation direction also suggested a small amount of strain in the MoS_2 monolayer system.

Results of the PL measurements, which are more sensitive to strain due to the funnel effect, revealed noticeable changes of the optical bandgap as a function of α (Fig. 1b). Strain due to the periodic substrate was determined using a reference value of 42 meV per 1% strain for the optical bandgap shift [29]. As shown in Fig. 1b, the difference between the PL peak at α = 0° and at α = 90° corresponds to a strain variation of 0% in MoS_2 on the flat sapphire substrate and 0.16% and 0.21% for corrugated substrates with periods of 180 nm and 250 nm, respectively. For samples on the two corrugated substrates, the angle dependence of

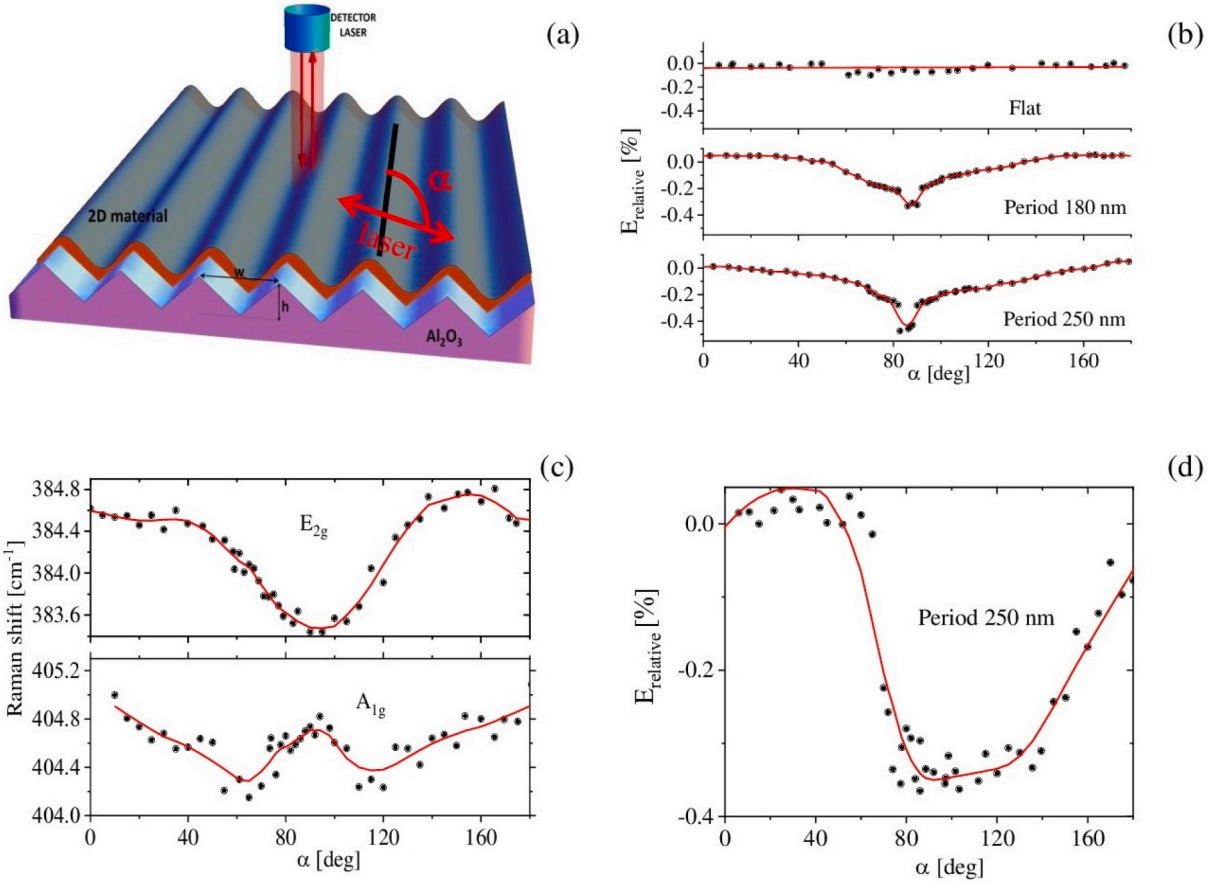

Fig. 1. Raman and PL experiments on a corrugated MoS_2 monolayer on Al_2O_3 substrate. (a) Schematic presentation of the laser and sample geometries. (b) Angle dependence of the relative optical bandgap energy of *polycrystalline* monolayer MoS_2 on corrugated (with 180-nm and 250-nm period) and flat substrates. (c) Angle dependence of the absolute value of Raman shifts of the E_{2g} and A_{1g} modes. (d) Relative optical bandgap energy ($E_{relative}$) for the single crystalline MoS_2 monolayer onto a corrugated sapphire with 250-nm periodicity.

the optical bandgap was clearly visible [11,29,30]. Considering that PL measurements provide information about the minimum value of the bandgap (which corresponds to maximum strain) and that regions of maximum local strain correspond to the regions of maximum topographic curvature [40,41,42] we assumed that the largest value of strain in the corrugated samples was directionally perpendicular to the corrugation direction.

Contrary to the polycrystalline MoS_2 monolayer results, the single-crystal MoS_2 monolayer on a corrugated sapphire substrate showed anomalies in the angle dependence of the A_{1g} and E_{2g} Raman modes (Fig. 1c). The difference between Raman shifts at $\alpha = 0^\circ$ and $\alpha = 90^\circ$ of the E_{2g} mode was 1.1 cm^{-1}, which corresponds to ~0.25% strain (Fig. 1b). The A_{1g} peak also exhibits a small Raman shift with variations of the α value (Fig. 1d). Using the optical bandgap shift at the same angles, strain on the single-crystal MoS_2 monolayer was determined to be ~0.22% (Fig. 1d) [10].

The polarization–resolved second harmonic generation (SHG) measurements allowed us to test the assumption for the strain on the sample by imaging the two-dimensional strain field in MoS_2 [43]. Polarization-resolved SHG data collected from the single-crystal MoS_2 monolayers on corrugated sapphire substrates (250–nm period) confirmed the strain orientation in the samples, with a maximum largest value at $\alpha = 90^0$ with respect to the corrugation direction (Fig. 2). Strain values derived from SHG measurements agree remarkably well with those from micro-Raman and PL measurements (Table S3).

Our aforementioned results reveal that periodic nanostructures imposed by the corrugated substrates introduce nanometre-scaled, orientational strain on the polycrystaline and single-crystal MoS_2 monolayers. The micro-Raman results of the corrugated MoS_2 monolayer allowed us to determine its maximal strain values ranging between 0.16% and 0.25%, depending on the corrugation period. Furthermore, comparisons between results from various sample preparations show that the transfer techniques used in our experiments did not introduce significant strain in the MoS_2 monolayers (Table S3). Absence of the E_{2g} mode splitting confirmed that the applied strain was small so the strain modification of the bandgap is linear (Figure S3).

Results of the SHG experiments (Fig. 2) illustrate that strain variation in the MoS_2 monolayers on corrugated sapphire is non-uniform, with the largest % strain near $\alpha = 90^\circ$ with respect to the corrugation direction. Considering the funnel effect and consequent radiative recombination of bright excitons, one could expect large values of the PL intensities on the peaks of the corrugation. However, we observed a reduction of the PL intensities at an angle of 90° compared to those at 0° (Fig. 3a). Supplementary AFM and SNOM measurements of polycrystalline MoS_2 monolayer show that the largest intensity of emitted light was observed in troughs of the corrugation, instead of the peaks (Fig. 3b and c, respectively). We should emphasize that SNOM experiments work below the diffraction limit so an increase in the collected light emissions comes from excitons' recombination and would not be interfered by light constructive interference effect.

To explain the phenomenon observed in SHG and SNOM experiments, we consider two possible effects of strain on the band structure of the MoS_2 monolayer: modulation of the bandgap width (the funnel effect) and splitting of the conduction and/or valence bands [15]. The implication of the first effect is a tuneability of the optical bandgap as presented in Fig. 1a-b. The largest change of the bandgap observed was 0.4% at $\alpha = 90^o$with respect to the corrugation direction for both polycrystalline and single-crystal MoS_2 monolayers. The second effect is more complex. In monolayer TMDs, the conduction band minima and valence band maxima are located at the degenerate +K and −K points at the corners of the hexagonal Brillouin zone. The +K and −K valleys are time reversals of one another. The conduction band is comprised mainly of d_z-orbitals whereas the valence band is comprised of $d_{x^2-y^2} \pm id_{xy}$ orbitals. As a result, strong spin–orbit coupling (SOC) from the dominant metal d_z –orbitals leads to a large spin splitting in the valence band (up to 150 meV) in the z-direction. In other words, the SOC lifts the spin

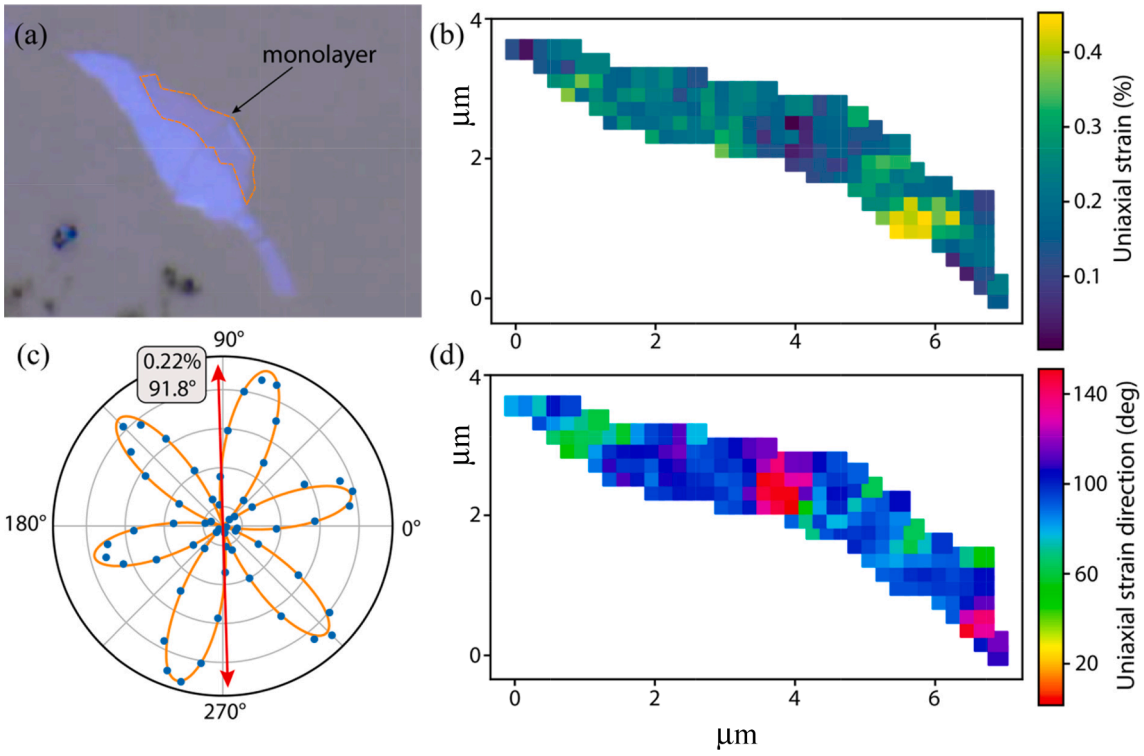

Fig. 2. (a) An optical image of a single-crystal MoS_2 monolayer transferred onto a corrugated sapphire substrate (250-nm period). (b) Map of uniaxial strain values in % strain of the sample. (c) Polarization-resolved SHG intensity (symbols: measurement data; line: fit). The SHG intensity pattern corresponds to a strain magnitude of 0.22% in 91.8° direction. The red arrow indicates the fitted uniaxial strain direction. (d) Map of uniaxial strain direction α in the MoS_2 with respect to the corrugation direction.

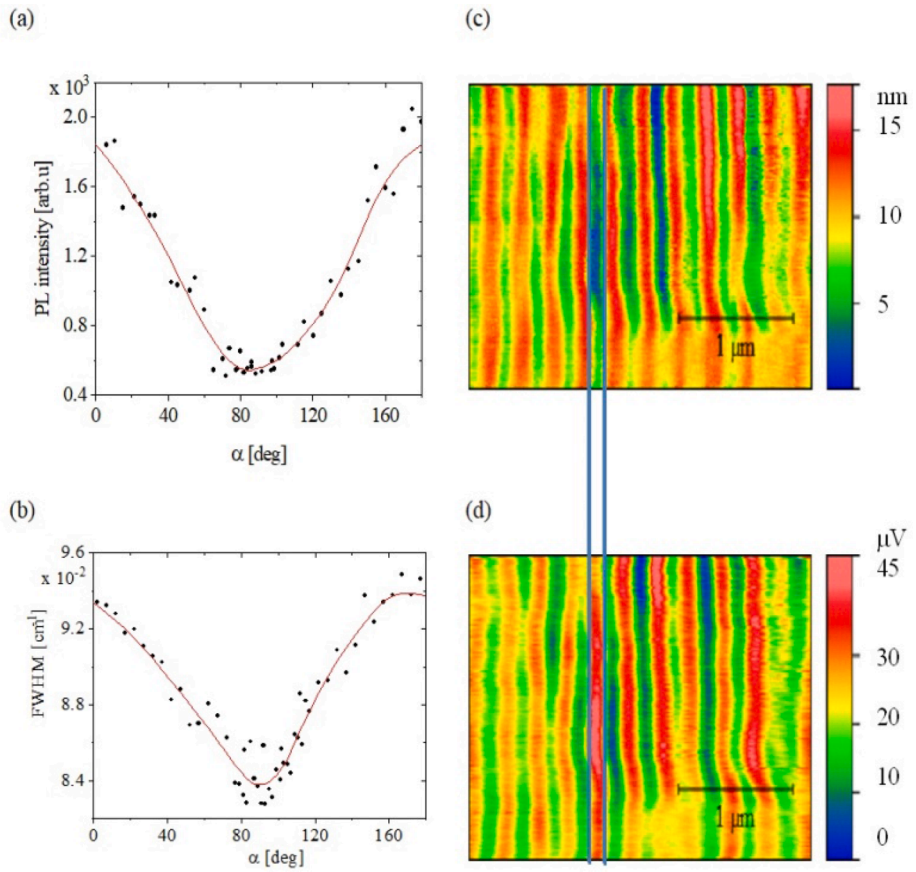

Fig. 3. Angle dependence of PL intensity (a) and FWHM (b) of the optical bandgap of a single-crystal MoS_2 monolayer on a corrugated surface. AFM topography (c) and SNOM (d) results collected from a polycrystalline MoS_2 monolayer. Both single-crystal and polycrystalline MoS_2 were transferred onto a corrugated sapphire substrate with a periodicity of 250 nm. The vertical violet lines show the distance shift between topography and SNOM pictures.

degeneracy of the energy bands due to breaking of the inversion symmetry. For the conduction band, the metal d_z-orbitals do not contribute to the SOC, so that the band splitting is much smaller (-3 meV) [15].

Recent investigation revealed that the dark excitons appear at 14 meV below the bright ones [16]. Symmetry breaking by strain application can remove the degeneracy at ±K and enable scattering from bright to dark excitons when combined with the spin relaxation phenomenon. Moreover, application of tensile strain on the monolayer reduces the separation energy between bright and dark excitons [4]. Such process is related with the spin-flip of an electron or a hole of an exciton.

Based on a previous theoretical study [27], the coupling between the spin and local angular momentum includes interaction of electrons with both the static surface wrinkles and phonons. Spin-flip mechanisms in a variety of processes are often attributed to the electron phonon scattering mechanism. However, the full width at half maximum (FWHM) of optical bandgaps of polycrystalline MoS_2 samples showed minimum values near $\alpha = 90°$ (Fig. 3c), which suggests that the electron–phonon scattering process does not drive the spin-flip mechanism in this system. Therefore, we conclude that the spin-relaxation mechanism is related with the spin coupling with local curvature, which can be associated with the corrugated sapphire substrate. Considering the lateral sizes of corrugated sapphire substrates of q^{-1} and a mean-free path of electrons l, one can estimate the contribution of ballistic or inelastic processes to the relaxation time. Following the model introduced in [27] that shows the diffusive and ballistic components of an electron's relaxation time for $q^{-1} = 250$ nm and $l = 3$ nm [44], we get $ql \ll 1$, what indicates a suppression of ballistic component of the total relaxation time.

Our interpretation of the results presented in Fig. 3 – which illustrates the lower PL and SNOM intensities at the peaks of the nanostructure – is based on a bright to dark exciton conversion process. Due to the funnel effect, bright excitons excited by laser light migrate to regions with a maximum strain before recombination, but this strain also splits the conduction band [4]. Deformation of the MoS_2 monolayer surface by the corrugated substrate modulates the atomic positions, thus changing the atomic interactions and orbital hybridizations, which ultimately lead to an electron or hole spin-flip [45], as illustrated in Fig. 4. Therefore, we hypothesize that the spin-flip mechanism is responsible for the conversion from bright to dark excitons, rather than the electron phonon scattering mechanism. According to [45], out-of-plane deformations, such as the corrugation in the MoS_2 system, generate additional Rashba–like contributions to the SOC of the MoS_2 and enhance the spin-flip scattering process. The spin-flip process is more probable in the conduction band due to the much smaller values of the band splitting.

The exciton conversion hypothesis can also be supported by results of SNOM experiments. As mentioned in the introductory section, a bright exciton (the electron and the hole have parallel spins) can recombine easily through the emission of a photon but a dark exciton (the spins are antiparallel) cannot recombine via direct emission of a photon as this would not allow for the spin momentum conservation. The largest intensity of light measured by SNOM was recorded in direction parallel to the corrugation direction, i.e. in direction in which the spin-flip doesn't occur. These also help explain the bright-to-dark exciton conversion hypothesis.

5. Conclusions

Our results demonstrate that application of periodic uniaxial strains

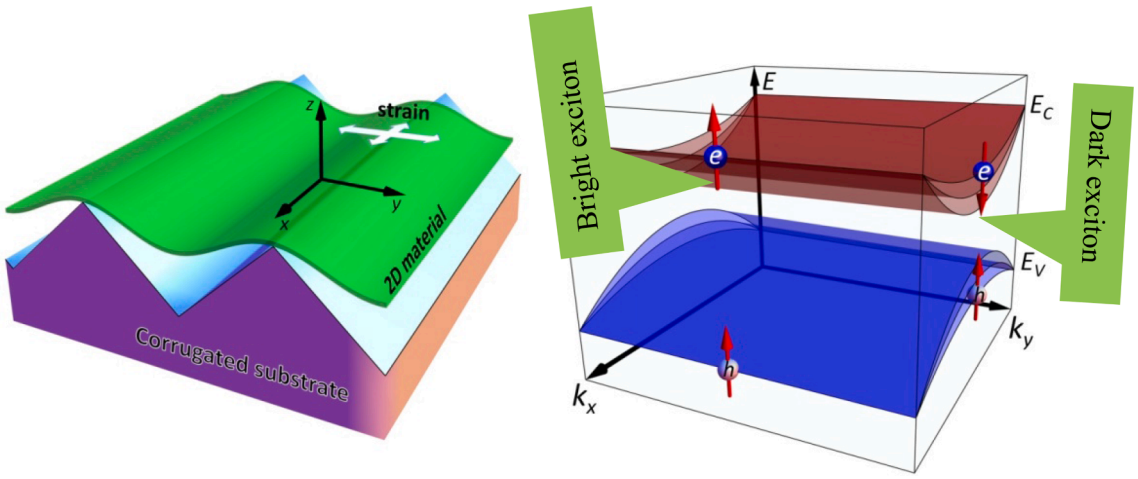

Fig. 4. An illustration of the strain orientation in the monolayer MoS_2 and a model of band splitting and bandgap modifications of the spin-flip mechanism for two-dimensional MoS_2 monolayer subjected to a periodic strain.

on two-dimensional materials such as MoS_2 monolayer can be an effective means to modify their electronic and optical properties in submicron scales. The application of the periodic strain on both polycrystalline and single-crystal MoS_2 monolayers results in significant bandgap modifications – a property advantageous in photovoltaic applications, as it enables conversion of a wider range of wavelengths into electric currents. Since excitons must be collected before recombination to facilitate energy harvesting, another important requirement for photovoltaic applications is long exciton lifetimes. Bright exciton lifetimes are shorter than their dark exciton counterparts, so conversion from bright to dark excitons is highly desirable in the photovoltaic applications. Our results reveal that the strain from the corrugated sapphire substrate has two effects on the charge transport of the MoS_2 monolayer: lifting band degeneracy at K points of the Brillouin zone and reduction of the spin-relaxation time due to the spin–lattice coupling. We also have shown that the spin–lattice coupling is mainly due to the spin coupling with the corrugated surface, but the spin coupling with phonons is negligible. These two effects can promote the light to dark exciton conversion.

The conversion efficiency can be further enhanced by a reduction in the separation energy between light and dark excitons due to tensile strain. Based on our angle-dependent PL and SNOM intensities of the MoS_2 monolayers, we conclude that the spin-flip scattering process is more probable in the conduction band due to much smaller values of the band splitting. Future studies using our approach on other TMDs and heterostructural monolayers can further shed light on the effects of periodic uniaxial strains on their transport properties and bandgaps as well as potential photovoltaic applications.

Declaration of Competing Interest

The authors declare that they have no known competing financial interests or personal relationships that could have appeared to influence the work reported in this paper.

Acknowledgment

M.W. acknowledges: the support of the Fulbright Senior Award 2016/2017 and grants of the Polish National Centre of Science: UMO-2016/21/B/ST3/00452, Ministry of Education and Science 7219/IA/SP/2021 as well as the LaSensA project carried out under the M-ERA.NET scheme and co-funded by the European Union's Horizon 2020 programme, the Research Council of Lithuania (LMTLT), agreement No. S-M-ERA.NET-21-2, the Saxon State Ministry for Science, Culture and Tourism (Germany) and the National Science Centre of Poland, project No. 2020/02/Y/ST5/00086 (MW+JJ). D.A. acknowledges the support of the Lybarger Endowed Faculty Fellowship, the Fulbright Specialist Award, and the Presidential Early Career Award for Scientists and Engineers (PECASE) through the Army Research Office.

The work was partly done at the Texas Nanofabrication Facility supported by NSF grant NNCI-1542159

Appendix A. Supplementary material

Supplementary data to this article can be found online at https://doi.org/10.1016/j.apsusc.2022.154078.

References

[1] D. Akinwande, N. Petrone, J. Hone, Two-dimensional flexible nanoelectronics, Nat. Commun. 5 (2014) 1–12, https://doi.org/10.1038/ncomms6678.
[2] S. Kabiri Ameri, R. Ho, H. Jang, L.i. Tao, Y. Wang, L. Wang, D.M. Schnyer, D. Akinwande, N. Lu, Graphene electronic tattoo sensors, ACS Nano 11 (8) (2017) 7634–7641.
[3] H. Wang, C. Zhang, W. Chan, C. Manolatou, S. Tiwari, F. Rana, Radiative lifetimes of excitons and trions in monolayers of the metal dichalcogenide MoS_2, Phys. Rev. B. 93 (2016), 045407, https://doi.org/10.1103/PhysRevB.93.045407.
[4] M. Feierabend, Z. Khatibi, G. Berghäuser, E. Malic, Dark exciton based strain sensing in tungsten-based transition metal dichalcogenides, Phys. Rev. B. 99 (2019), 195454, https://doi.org/10.1103/PhysRevB.99.195454.
[5] C. Robert, D. Lagarde, F. Cadiz, G. Wang, B. Lassagne, T. Amand, A. Balocchi, P. Renucci, S. Tongay, B. Urbaszek, X. Marie, Exciton radiative lifetime in transition metal dichalcogenide monolayers, Phys. Rev. B. 93 (2016), 205423, https://doi.org/10.1103/PhysRevB.93.205423.
[6] T. Mueller, E. Malic, Exciton physics and device application of two-dimensional transition metal dichalcogenide semiconductors, Npj 2D Mater Appl. 2 (2018) 29, https://doi.org/10.1038/s41699-018-0074-2.
[7] D. Akinwande, C.J. Brennan, J.S. Bunch, P. Egberts, J.R. Felts, H. Gao, R. Huang, J. S. Kim, T. Li, Y. Li, K.M. Liechti, N. Lu, H.S. Park, E.J. Reed, P. Wang, B. I. Yakobson, T. Zhang, Y.W. Zhang, Y. Zhou, Y. Zhu, A review on mechanics and mechanical properties of 2D materials—graphene and beyond, Extrem. Mech. Lett. 13 (2017) 42–77, https://doi.org/10.1016/j.eml.2017.01.008.
[8] K. Liu, Q. Yan, M. Chen, W. Fan, Y. Sun, J. Suh, D. Fu, S. Lee, J. Zhou, S. Tongay, J. Ji, J.B. Neaton, J. Wu, Elastic properties of chemical-vapor-deposited monolayer MoS_2, WS_2, and their bilayer heterostructures, Nano Lett. 14 (9) (2014) 5097–5103, https://doi.org/10.1021/nl501793a.
[9] M.-L. Tsai, S.-H. Su, J.-K. Chang, D.-S. Tsai, C.-H. Chen, C.-I. Wu, L.-J. Li, L.-J. Chen, J.-H. He, Monolayer MoS_2 heterojunction solar cells, ACS Nano 8 (8) (2014) 8317–8322, https://doi.org/10.1021/nn502776h.
[10] H.J. Conley, B. Wang, J.I. Ziegler, R.F. Haglund, S.T. Pantelides, K.I. Bolotin, Bandgap engineering of strained monolayer and bilayer MoS_2, Nano Lett. 13 (8) (2013) 3626–3630, https://doi.org/10.1021/nl4014748.
[11] A. Castellanos-Gomez, R. Roldán, E. Cappelluti, M. Buscema, F. Guinea, H.S.J. van der Zant, G.A. Steele, Local strain engineering in atomically thin MoS_2, Nano Lett. 13 (11) (2013) 5361–5366, https://doi.org/10.1021/nl402875m.
[12] D. Lloyd, X. Liu, J.W. Christopher, L. Cantley, A. Wadehra, B.L. Kim, B.B. Goldberg, A.K. Swan, J.S. Bunch, Band gap engineering with ultralarge biaxial strains in suspended monolayer MoS_2, Nano Lett. 16 (9) (2016) 5836–5841, https://doi.org/10.1021/acs.nanolett.6b0261510.1021/acs.nanolett.6b02615.s001.

[13] T. Cheiwchanchamnangij, W.R.L. Lambrecht, Y. Song, H. Dery, Strain effects on the spin-orbit-induced band structure splittings in monolayer MoS_2 and graphene, Phys. Rev. B - Condens. Matter Mater. Phys. 88 (2013), 155404, https://doi.org/10.1103/PhysRevB.88.155404.
[14] M. Baranowski, A. Surrente, D.K. Maude, M. Ballottin, A.A. Mitioglu, P.C. M. Christianen, Y.C. Kung, D. Dumcenco, A. Kis, P. Plochocka, Dark excitons and the elusive valley polarization in transition metal dichalcogenides, 2D Mater. 4 (2) (2017) 025016, https://doi.org/10.1088/2053-1583/aa58a0.
[15] H. Yu, X. Cui, X. Xu, W. Yao, Valley excitons in two-dimensional semiconductors, Natl. Sci. Rev. 2 (2015) 57–70, https://doi.org/10.1093/nsr/nwu078.
[16] C. Robert, B. Han, P. Kapuscinski, A. Delhomme, C. Faugeras, T. Amand, M. R. Molas, M. Bartos, K. Watanabe, T. Taniguchi, B. Urbaszek, M. Potemski, X. Marie, Measurement of the spin-forbidden dark excitons in MoS_2 and $MoSe_2$ monolayers, Nat. Commun. 111 (11) (2020) 1–8, https://doi.org/10.1038/s41467-020-17608-4.
[17] W.S. Yun, S.W. Han, S.C. Hong, I.G. Kim, J.D. Lee, Thickness and strain effects on electronic structures of transition metal dichalcogenides: 2H-MX_2 semiconductors (M = Mo, W; X = S, Se, Te), Phys. Rev. B - Condens. Matter Mater. Phys. 85 (2012), 033305, https://doi.org/10.1103/PhysRevB.85.033305.
[18] L. Zeng, Z. Xin, P. Chang, X. Liu, Strain effects on monolayer MoS_2 field effect transistors, Jpn. J. Appl. Phys. 54 (4S) (2015), 04DC17, https://doi.org/10.7567/JJAP.54.04DC17.
[19] C.V. Nguyen, V.V. Ilyasov, H.V. Nguyen, H.N. Nguyen, Band gap and electronic properties of molybdenum disulphide under strain engineering: density functional theory calculations, Mol. Simul. 43 (2) (2017) 86–91, https://doi.org/10.1080/08927022.2016.1233549.
[20] I. Niehues, R. Schmidt, M. Drüppel, P. Marauhn, D. Christiansen, M. Selig, G. Berghäuser, D. Wigger, R. Schneider, L. Braasch, R. Koch, A. Castellanos-Gomez, T. Kuhn, A. Knorr, E. Malic, M. Rohlfing, S. Michaelis de Vasconcellos, R. Bratschitsch, Strain control of exciton-phonon coupling in atomically thin semiconductors, Nano Lett. 18 (3) (2018) 1751–1757, https://doi.org/10.1021/acs.nanolett.7b0486810.1021/acs.nanolett.7b04868.s001.
[21] Y. Chai, S. Su, D. Yan, M. Ozkan, R. Lake, C.S. Ozkan, Strain gated bilayer molybdenum disulfide field effect transistor with edge contacts, Sci. Rep. 7 (2017) 1–9, https://doi.org/10.1038/srep41593.
[22] W. Wu, L. Wang, R. Yu, Y. Liu, S.-H. Wei, J. Hone, Z.L. Wang, Piezophototronic effect in single-atomic-layer MoS_2 for strain-gated flexible optoelectronics, Adv. Mater. 28 (38) (2016) 8463–8468, https://doi.org/10.1002/adma.201602854.
[23] W. Wu, L. Wang, Y. Li, F. Zhang, L. Lin, S. Niu, D. Chenet, X. Zhang, Y. Hao, T. F. Heinz, J. Hone, Z.L. Wang, Piezoelectricity of single-atomic-layer MoS_2 for energy conversion and piezotronics, Nature 514 (7523) (2014) 470–474, https://doi.org/10.1038/nature13792.
[24] X. Zhou, J. Shi, Y. Qi, M. Liu, D. Ma, Y.u. Zhang, Q. Ji, Z. Zhang, C. Li, Z. Liu, Y. Zhang, Periodic modulation of the doping level in striped MoS_2 superstructures, ACS Nano 10 (3) (2016) 3461–3468, https://doi.org/10.1021/acsnano.5b07545.
[25] C.R. Zhu, G. Wang, B.L. Liu, X. Marie, X.F. Qiao, X. Zhang, X.X. Wu, H. Fan, P. H. Tan, T. Amand, B. Urbaszek, Strain tuning of optical emission energy and polarization in monolayer and bilayer MoS_2, Phys. Rev. B - Condens. Matter Mater. Phys. 88 (2013), 121301, https://doi.org/10.1103/PhysRevB.88.121301.
[26] L. Yang, X. Cui, J. Zhang, K. Wang, M. Shen, S. Zeng, S.A. Dayeh, L. Feng, B. Xiang, Lattice strain effects on the optical properties of MoS_2 nanosheets, Sci. Rep. 4 (2014) 1–7, https://doi.org/10.1038/srep05649.
[27] H. Ochoa, F. Guinea, V.I. Fal'Ko, Spin memory and spin-lattice relaxation in two-dimensional hexagonal crystals, Phys. Rev. B - Condens. Matter Mater. Phys. 88 (2013), 195417, https://doi.org/10.1103/PHYSREVB.88.195417/FIGURES/3/MEDIUM.
[28] B.G. Shin, G.H. Han, S.J. Yun, H.M. Oh, J.J. Bae, Y.J. Song, C.-Y. Park, Y.H. Lee, Indirect bandgap puddles in monolayer MoS_2 by substrate-induced local strain, Adv. Mater. 28 (42) (2016) 9378–9384, https://doi.org/10.1002/adma.201602626.
[29] H. Li, A.W. Contryman, X. Qian, S.M. Ardakani, Y. Gong, X. Wang, J.M. Weisse, C. H. Lee, J. Zhao, P.M. Ajayan, J. Li, H.C. Manoharan, X. Zheng, Optoelectronic crystal of artificial atoms in strain-textured molybdenum disulphide, Nat. Commun. 6 (2015) 1–7, https://doi.org/10.1038/ncomms8381.
[30] V.S. Mangu, M. Zamiri, S.R.J. Brueck, F. Cavallo, Strain engineering, efficient excitonic photoluminescence, and exciton funnelling in unmodified MoS_2 nanosheets, Nanoscale. 9 (43) (2017) 16602–16606.
[31] J.i. Feng, X. Qian, C.-W. Huang, J.u. Li, Strain-engineered artificial atom as a broad-spectrum solar energy funnel, Nat. Photonics. 6 (12) (2012) 866–872, https://doi.org/10.1038/nphoton.2012.285.
[32] A. Moghadasi, M.R. Roknabadi, S.R. Ghorbani, M. Modarresi, Electronic and phononic modulation of MoS_2 under biaxial strain, Phys. B Condens. Matter. 526 (2017) 96–101, https://doi.org/10.1016/j.physb.2017.09.059.
[33] R. Gabai, A. Ismach, E. Joselevich, Nanofacet lithography: a new bottom-up approach to nanopatterning and nanofabrication by soft replication of spontaneously faceted crystal surfaces, Adv. Mater. 19 (10) (2007) 1325–1330, https://doi.org/10.1002/adma.200601625.
[34] J. Jenczyk, E. Coy, S. Jurga, Poly(ethylene oxide)-block-polystyrene thin films morphology controlled by drying conditions and substrate topography, Eur. Polym. J. 75 (2016) 234–242, https://doi.org/10.1016/j.eurpolymj.2015.12.020.
[35] S. Park, D.H. Lee, J.i. Xu, B. Kim, S.W. Hong, U. Jeong, T. Xu, T.P. Russell, Macroscopic 10-terabit–per–square-inch arrays from block copolymers with lateral order, Science 323 (5917) (2009) 1030–1033.
[36] C. Rice, R.J. Young, R. Zan, U.B. al, Raman-scattering measurements and first-principles calculations of strain-induced phononshifts in monolayer MoS_2, Phys. Rev. B. 87 (n.d.) 81307.
[37] L. Su, Y. Zhang, Y. Yu, L. Cao, Dependence of coupling of quasi 2-D MoS_2 with substrates on substrate types, probed by temperature dependent Raman scattering, Nanoscale. 6 (9) (2014) 4920–4927.
[38] L. Liang, V. Meunier, First-principles Raman spectra of MoS_2, WS_2 and their heterostructures, Nanoscale. 6 (2014) 5394–5401, https://doi.org/10.1039/c3nr06906k.
[39] K.K.H.C.J.-U. Lee, Resonant Raman and photoluminescence spectra of suspended molybdenum disulphide, 2D Mater. 2 (n.d.) 44003.
[40] M. Rahaman, R.D. Rodriguez, G. Plechinger, S. Moras, C. Schüller, T. Korn, D.R. T. Zahn, Highly localized strain in a MoS_2/Au heterostructure revealed by tip-enhanced Raman spectroscopy, Nano Lett. 17 (10) (2017) 6027–6033, https://doi.org/10.1021/acs.nanolett.7b0232210.1021/acs.nanolett.7b02322.s001.
[41] Z. Zhang, A.C. De Palma, C.J. Brennan, G. Cossio, R. Ghosh, S.K. Banerjee, E.T. Yu, Probing nanoscale variations in strain and band structure of MoS_2 on Au nanopyramids using tip-enhanced Raman spectroscopy, Phys. Rev. B. 97 (2018), 085305, https://doi.org/10.1103/PhysRevB.97.085305.
[42] C. Li, B. Fan, W. Li, L. Wen, Y. Liu, T. Wang, K. Sheng, Y. Yin, Bandgap engineering of monolayer MoS_2 under strain: A DFT study, J. Korean Phys. Soc. 66 (11) (2015) 1789–1793, https://doi.org/10.3938/jkps.66.1789.
[43] L. Mennel, M.M. Furchi, S. Wachter, M. Paur, D.K. Polyushkin, T. Mueller, Optical imaging of strain in two-dimensional crystals, Nat. Commun. 9 (2018) 1–6, https://doi.org/10.1038/s41467-018-02830-y.
[44] K.K.H. Smithe, C.D. English, S.V. Suryavanshi, E. Pop, Intrinsic electrical transport and performance projections of synthetic monolayer MoS_2 devices, 2D Mater. 4 (1) (2016), 011009, https://doi.org/10.1088/2053-1583/4/1/011009.
[45] S.B. Touski, R. Roldán, M. Pourfath, M. Pilar López-Sancho, Enhanced spin-flip scattering by surface roughness in WS_2 and MoS_2 armchair nanoribbons, Phys. Rev. B. 95 (2017), 165301, https://doi.org/10.1103/PhysRevB.95.165301.